Higgs amplitude mode in massless Dirac fermion systems

Ming Lu,[1,2] Haiwen Liu,[1,2] Pei Wang,[1,3] and X. C. Xie[1,2]
[1]*International Center for Quantum Materials and School of Physics, Peking University, Beijing 100871, China*
[2]*Collaborative Innovation Center of Quantum Matter Beijing 100871, China*
[3]*Department of Physics, Zhejiang Normal University, Jinhua 321004, China*
(Received 9 December 2015; published 25 February 2016)

The Higgs amplitude mode in superconductors is the condensed-matter analogy of Higgs bosons in particle physics. We investigate the time evolution of Higgs amplitude mode in massless Dirac systems induced by a weak quench of an attractive interaction. We find that the Higgs amplitude mode in the half-filled honeycomb lattice has a logarithmic decaying behavior, qualitatively different from the $1/\sqrt{t}$ decay in the normal superconductors. Our study is also extended to the doped cases in honeycomb lattices. As for the three-dimensional Dirac semimetal at half filling, we obtain an undamped oscillation of the amplitude mode. Our finding is not only an important supplement to the previous theoretical studies on normal fermion systems but also provides an experimental signature to characterize the superconductivity in two- or three-dimensional Dirac systems.

DOI: 10.1103/PhysRevB.93.064516

I. INTRODUCTION

A conventional superconductor can be described by a charged complex order parameter $\Delta(r,t) = |\Delta(r,t)|e^{i\phi(r,t)}$. Its collective fluctuations around equilibrium include the oscillations of the phase and amplitude [1]. The phase mode, being coupled to the electromagnetic field, moves to a plasma frequency of the metal as a manifestation of the Anderson–Higgs mechanism [2–4]. The amplitude mode oscillates with angular frequency $2|\Delta_0|$, analogous to the "vibration" of the longitudinal component of the Higgs field in particle physics [5]. In this sense, the amplitude mode in superconductors is sometimes also called the Higgs mode or the Higgs amplitude mode in the literature [1,5–9].

The Higgs amplitude mode in superconductors, although theoretically predicted many years ago [10], has only been directly observed recently by the time-resolved terahertz (THz) pump-probe technique in a clean superconducting film [6,7], and by measuring the excess subgap optical conductance in disordered films near the superconductor-insulator phase transition [8]. The time evolution of the Higgs mode in the collisionless, dissipationless regime was studied intensely. It was revealed that the Higgs mode oscillates at a frequency of $2\Delta_\infty$ with a $1/\sqrt{t}$ decaying property in the weak-coupling limit, where Δ_∞ is the asymptotic value of the superconducting gap [9,11–13]. However, previous works all assume that the density of states (DOS) near the Fermi level is almost a constant within the Debye cutoff energy ω_D. This assumption obviously fails for honeycomb lattices or Dirac semimetals at half filling. Their DOS is either linear [two-dimensional (2D)] or quadratic [three-dimensional (3D)] at low energy, respectively, and vanishes at the Dirac point [14,15]. Since superconductivity is strongly affected by the DOS near the Fermi level [16], it would be theoretically interesting to study the time evolution of the Higgs mode in these systems. On the experimental side, the availability of the honeycomb optical lattice [17] and the tunable attractive interaction by Feshbach resonance [18] give a possible test ground for this study. Besides, the expected unique feature of the Higgs mode in a superconducting Dirac semimetal can be used as an important experimental characterization to distinguish it from normal superconductors [19,20].

In this paper, we study the quenched dynamics in the weak-coupling limit by using the Anderson pseudospin formalism [21]. We find that the Higgs mode has a log-decay behavior in the half-filled honeycomb lattice. To understand this behavior, we further study the pseudospins' phase dynamics and analytically solve the linearized equations of motion [9,11,13]. The doped cases are also studied numerically. In the low-doping limit, a double-frequency feature is found. The larger frequency increases noticeably and its peak broadens with the doping level. In the high-doping limit, we are back to the $1/\sqrt{t}$ decaying property, as in a normal superconductor. When considering the 3D Dirac semimetal at the neutral point, we find that the Higgs mode exhibits an undamped oscillation, with all the pseudospins precessing synchronously.

II. MODEL AND FORMALISM

We start by considering the negative-U Hubbard model on a honeycomb lattice:

$$\hat{H} = -\sum_{\langle ij\rangle,\sigma} \hat{a}^\dagger_{i\sigma} b_{j\sigma} + \text{H.c.} - U\sum_i \hat{n}_{i\uparrow}\hat{n}_{i\downarrow} - \mu\sum_{i\sigma}\hat{n}_{i\sigma}, \quad (1)$$

where $\hat{a}_i$ ($\hat{b}_i$) is the on-site annihilation operator on sublattice A (B), $\hat{n}_{i\sigma}$ is the number operator on lattice site i with spin index σ, μ is the chemical potential, and U is the the on-site attractive interaction. We choose nearest-neighbor hopping as the energy unit throughout this paper.

To study the dynamics, we write out the corresponding mean-field Hamiltonian in $\mathbf{k}$ space after a unitary transformation: $\hat{a}_{\mathbf{k}\sigma} = \frac{1}{\sqrt{2}}(e^{i\theta_\mathbf{k}}\hat{c}_{\mathbf{k}\sigma} + \hat{d}_{\mathbf{k}\sigma})$, $\hat{b}_{\mathbf{k}\sigma} = \frac{1}{\sqrt{2}}(-\hat{c}_{\mathbf{k}\sigma} + e^{-i\theta_\mathbf{k}}\hat{d}_{\mathbf{k}\sigma})$:

$$H_{\text{MF}} = -\sum_\mathbf{k}(\mu - |\gamma_\mathbf{k}|)\hat{c}^\dagger_{\mathbf{k}\sigma}c_{\mathbf{k}\sigma} - \sum_\mathbf{k}(\mu + |\gamma_\mathbf{k}|)\hat{d}^\dagger_{\mathbf{k}\sigma}d_{\mathbf{k}\sigma} - \Delta^*(t)\sum_\mathbf{k}(\hat{c}^\dagger_{\mathbf{k}\uparrow}c^\dagger_{-\mathbf{k}\downarrow} + \hat{d}^\dagger_{\mathbf{k}\uparrow}d^\dagger_{-\mathbf{k}\downarrow}) + \text{H.c.}, \quad (2)$$

where $\hat{a}_{\mathbf{k}\sigma}$ ($\hat{b}_{\mathbf{k}\sigma}$) is the Fourier component of $\hat{a}_i$ ($\hat{b}_i$), $e^{i\theta_\mathbf{k}} = \gamma_\mathbf{k}/|\gamma_\mathbf{k}|$ with $\gamma_\mathbf{k} = \sum_\mathbf{k} e^{i\mathbf{k}\cdot\boldsymbol{\delta}}$ and $\boldsymbol{\delta}$ being the three real-space nearest-neighbor vectors, the time-dependent order parameter $\Delta(t) = \frac{U}{N_c}\sum_\mathbf{k}\langle a^\dagger_{\mathbf{k}\uparrow}a^\dagger_{-\mathbf{k}\downarrow}\rangle = \frac{U}{N_c}\sum_\mathbf{k}\langle b^\dagger_{\mathbf{k}\uparrow}b^\dagger_{-\mathbf{k}\downarrow}\rangle$, in which N_c is

 ©2016 American Physical Society

the number of unit cells and $\langle\cdots\rangle$ denotes the time-dependent quantum-mechanical expectation value.

We define two sets of Anderson pseudospins:

$$\hat{\boldsymbol{S}}_{\boldsymbol{k}}^{(+)} = \frac{1}{2}(\hat{c}_{\boldsymbol{k}\uparrow}^{\dagger}, \hat{c}_{-\boldsymbol{k}\downarrow})\boldsymbol{\sigma}\begin{pmatrix}\hat{c}_{\boldsymbol{k}\uparrow}\\ \hat{c}_{-\boldsymbol{k}\downarrow}^{\dagger}\end{pmatrix},$$

$$\hat{\boldsymbol{S}}_{\boldsymbol{k}}^{(-)} = \frac{1}{2}(\hat{d}_{\boldsymbol{k}\uparrow}^{\dagger}, \hat{d}_{-\boldsymbol{k}\downarrow})\boldsymbol{\sigma}\begin{pmatrix}\hat{d}_{\boldsymbol{k}\uparrow}\\ \hat{d}_{-\boldsymbol{k}\downarrow}^{\dagger}\end{pmatrix},$$

with their corresponding local fields $\boldsymbol{b}_{\boldsymbol{k}}^{(\pm)}(t) = (\Delta^{\mathrm{R}}(t), \Delta^{\mathrm{I}}(t), \mu \mp |\gamma_{\mathbf{k}}|)$. It is straightforward to check that the pseudospin operators satisfies the commutation relationship of the angular momentum (with $\hbar = 1$). By using the above definition, the Hamiltonian can be written as the sum of the "Zeeman energy" of pseudospins in their corresponding local fields:

$$H_{\mathrm{MF}} = -2\sum_{\mathbf{k},i=\pm}\boldsymbol{b}_{\mathbf{k}}^{(i)}\cdot\hat{\boldsymbol{S}}_{\boldsymbol{k}}^{(i)}. \tag{3}$$

From the Hamiltonian, we can get the equations of motion of pseudospins: $\frac{\partial}{\partial t}\boldsymbol{S}_{\boldsymbol{k}}^{(i)}(t) = -2\boldsymbol{b}_{\boldsymbol{k}}^{(i)}\times\boldsymbol{S}_{\boldsymbol{k}}^{(i)}(t)$, where $i = \pm$ and $\boldsymbol{S}_{\boldsymbol{k}}^{(i)}(t) \equiv \langle\hat{\boldsymbol{S}}_{\boldsymbol{k}}^{(i)}\rangle$ are the expectation values of the Anderson pseudospin operators. The time-dependent gap can be written by using pseudospins as

$$\Delta(t) = \frac{U}{2N_c}\sum_{\boldsymbol{k},i=\pm}\left(S_{\boldsymbol{k}}^{(i)x} + iS_{\boldsymbol{k}}^{(i)y}\right).$$

For simplicity, we can also label the pseudospins by energy state ϵ_j rather than $\mathbf{k}$, so that we can combine the two sets of pseudospins as a single set. Explicitly, the equations of motion and time-dependent gap can be rewritten as

$$\frac{\partial}{\partial t}\boldsymbol{S}_j(t) = -2\boldsymbol{b}_j(t)\times\boldsymbol{S}_j(t), \tag{4}$$

$$\Delta(t) = \frac{U}{2N_c}\sum_j\left[S_j^x(t) + iS_j^y(t)\right], \tag{5}$$

with

$$\boldsymbol{b}_j(t) = (\Delta^R(t), \Delta^I(t), \epsilon_j), \tag{6}$$

where $\epsilon_j \in (-\omega_D, \omega_D)$, and $\boldsymbol{S}_j$ can be viewed as the classical spin with length $\frac{1}{2}$. Writing like this, the additional DOS information is needed. It satisfies $D(\epsilon) \propto |\epsilon - \mu|$, for we have a 2D linear dispersion near the Dirac point before superconducting; see Fig. 1(c).

The quenched dynamics is as follows: at $t \leqslant 0$, the system is in equilibrium with the initial interacting strength U_i. From the spin Hamiltonian, the initial spins are parallel to their local fields [Fig. 1(a)]. At $t = 0^+$, we change the interaction strength to U_f, then the local fields change immediately for the sudden change of $\Delta(t)$. Therefore, the current spin configuration is no longer stable. According to Eq. (4), they will precess around their local fields [Fig. 1(b)], which in turn will change the gap and the local fields simultaneously by Eqs. (5) and (6). We denote Δ_{0i} and Δ_{0f} as the corresponding equilibrium gap when the interaction strengths are U_i and U_f, respectively. In the following, they are used to describe the quenched dynamics for convenience.

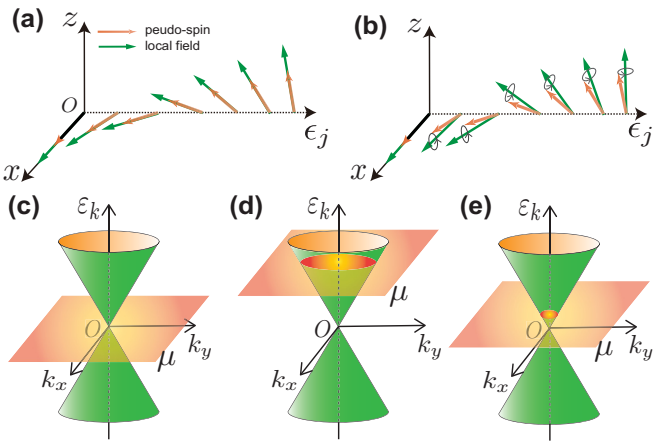

FIG. 1. Quenched dynamics illustration and three doping cases for honeycomb lattice. (a) When $t \leqslant 0$, the system is in the BCS ground state, and the pseudospins align in the direction of their local fields. (b) At $t = 0^+$, we change the interaction strength abruptly to force the system out of equilibrium. The pseudospins start to precess around their local fields, while the local fields also change due to their dependence on pseudospins. (c) The half-filling case $\mu = 0$, where $\varepsilon_{\boldsymbol{k}} \equiv \pm|\gamma_{\boldsymbol{k}}|$. (d) The high-doping limit $\mu \gg \Delta_{0f}$. (e) The low-doping limit $\mu \sim \Delta_{0f}$.

III. THREE DOPING CASES FOR HONEYCOMB LATTICE

We consider the dynamics of three doping cases for a honeycomb lattice as shown in Figs. 1(c)–1(e): half-filled, high-doping limit, and low-doping limit.

A. Half filled

Without loss of generality, we choose the initial gap Δ_{0i} to be real. The particle-hole symmetry guarantees the gap to be real throughout the evolution [12]. The problem is to solve a system of coupled differential equations (4) with the initial condition

$$\boldsymbol{S}_j(0) = \left(\frac{\Delta_{0i}}{2\sqrt{\Delta_{0i}^2 + \epsilon_j^2}}, 0, \frac{\epsilon_j}{2\sqrt{\Delta_{0i}^2 + \epsilon_j^2}}\right),$$

where in this case the gap and local fields are related with the pseudospins as $\Delta(t) = \frac{U_f}{2N_c}\sum_j S_j^x(t)$ and $\boldsymbol{b}_j(t) = (\Delta(t), 0, \epsilon_j)$. The DOS in the half-filling case is proportional to $|\epsilon|$.

We numerically simulate Eq. (4) with $N = 50\,000$ energy levels and the Debye cutoff energy $\omega_D = 0.5$. The method we use is the Runge–Kutta of the eighth order with an adjustable time step to have sufficiently high precision. We also tried other numbers of energy levels to verify that the results are unaffected by the finite-size effect. We also adopt the weak-coupling limit ($\Delta_{0f} \ll \omega_D$) and the weak-quench limit ($\delta\Delta_0 \equiv \Delta_{0i} - \Delta_{0f} \ll \Delta_{0f}$). To satisfy this, we quench from $\Delta_{0i} = 0.013$ to $\Delta_{0f} = 0.012$. The result is shown in Fig. 2: the data are well fit by a log-decay function:

$$\frac{\Delta(t)}{\Delta_{0f}} = a + \frac{2b\delta\Delta_0}{\Delta_{0f}}\frac{\cos(c\Delta_{0f}t + d)}{\ln(e\Delta_{0f}t)}. \tag{7}$$

The envelope functions $a \pm 2b\delta\Delta_0/\Delta_{0f}\ln(e\Delta_{0f}t)$ are used for indicating the log-decay behavior.

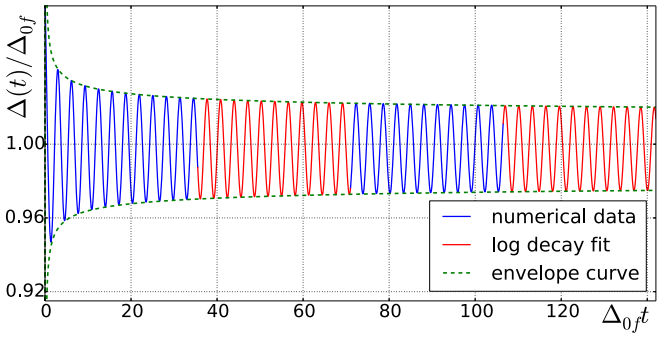

FIG. 2. Half filling. The numerical data (blue) obtained from simulating $N = 50\,000$ energy levels for $\Delta_{0i} = 0.013$ and $\Delta_{0f} = 0.012$, with Debye energy $\omega_D = 0.5$. The red curve is the fit by Eq. (7), while the green dotted lines are the envelope curves.

The fitted parameters are $a = 0.9975$, $b = 1.091$, $c = 1.994$, $d = 0.2554$, $e = 22.36$. We find that $c = 2a$ is almost exactly satisfied, which means that $\Delta(t)$ oscillates with the $2\Delta_\infty$ angular frequency, indicating that it is the Higgs amplitude mode. However, the mode has a logarithmic-decaying property in the present case, while it decays as $1/\sqrt{t}$ in normal superconductors. This slow-decaying behavior suggests that the Higgs mode in the half-filled superconducting honeycomb lattice has a much longer lifetime than that in the usual superconductors [22]. We also note that a is slightly smaller than 1, meaning $\Delta_\infty < \Delta_{0f}$. Explicitly, we find $1 - a \approx \delta\Delta_0^2/3\Delta_{0f}^2$. The similar behavior has been pointed out in previous publications for normal superconductors, claiming that the difference is of the order of $\delta\Delta_0^2/6\Delta_{0f}^2$ [13,23].

The slower decaying property compared with normal superconductors can be qualitatively understood by studying the phase dynamics of the single pseudospins on different energy levels [12]. Explicitly, we numerically calculate the precession angle $\phi_j(t)$ of pseudospin $\boldsymbol{S}_j$ around the time-independent vector $\boldsymbol{b}_j^\infty \equiv (\Delta_\infty, 0, \epsilon_j)$. As shown in Fig. 3(a), in the long-time limit, the phase becomes linear with respect to time so that we can characterize the precession frequency by the time-averaged frequency $\omega_j = \langle\omega_j(t)\rangle = [\phi_j(t_{\max}) - \phi_j(0)]/t_{\max}$. In Fig. 3(b), we compare ω_j for constant and linear DOS. For constant DOS, ω_j is equal to the quasiparticle spectrum $2(\Delta_\infty^2 + \epsilon_j^2)^{1/2}$. In the region when $\epsilon_j \lesssim 2\Delta_{0f}$, ω_j for both cases coincide with each other. However in the higher-energy region, ω_j for a linear DOS is much flatter than that for a constant DOS. The decaying of the amplitude is due to the dephasing mechanism for the precession of pseudospins. The flatter dispersion of ω_j represents a more synchronized precession of the pseudospins, resulting in a slower decaying of the amplitude.

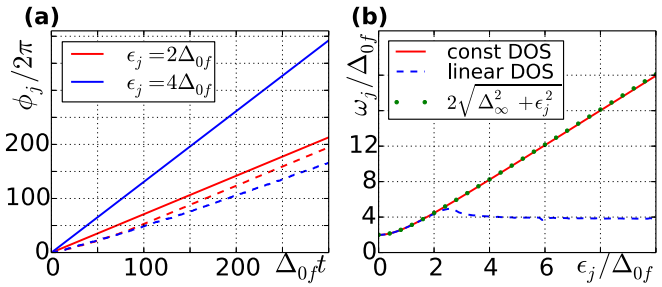

FIG. 3. Phase dynamics for $\Delta_{0i} = 0.013$ and $\Delta_{0f} = 0.012$ at half filling. The solid lines are for $D(\epsilon) = 1$, while the dashed lines are for $D(\epsilon) \propto |\epsilon|$. (a). The precession phases ϕ_j for $\epsilon_j = 2\Delta_{0f}, 4\Delta_{0f}$. They are almost linear for the large time dynamics and ϕ_j for constant DOS has larger "phase slope." (b). The time averaged precession frequency ω_j. For constant DOS, ω_j coincides with quasiparticle energy spectrum. For linear DOS case, the flatter ω_j's dispersion gives rise to in a weaker dephasing, therefore a slower decay of the amplitude.

To quantitatively understand the fitting equation (7), we solve equations of motion (4) by linearizing it around

$$\boldsymbol{S}_j^f \equiv \left(\frac{\Delta_{0f}}{2\sqrt{\Delta_{0f}^2 + \epsilon_j^2}}, 0, \frac{\epsilon_j}{2\sqrt{\Delta_{0f}^2 + \epsilon_j^2}}\right)$$

and $\boldsymbol{b}_j^f \equiv (\Delta_{0f}, 0, \epsilon_j)$:

$$\begin{aligned}
\frac{\partial}{\partial t}\delta S_j^x(t) &= 2\epsilon_j \delta S_j^y(t), \\
\frac{\partial}{\partial t}\delta S_j^y(t) &= \frac{\epsilon_j}{\sqrt{\Delta_{0f}^2 + \epsilon_j^2}}\delta\Delta(t) + 2\Delta_{0f}\delta S_j^z(t) - 2\epsilon_j \delta S_j^x(t), \\
\frac{\partial}{\partial t}\delta S_j^z(t) &= -2\Delta_{0f}\delta S_j^y(t),
\end{aligned} \tag{8}$$

where $\delta\Delta(t) \equiv \Delta(t) - \Delta_{0f}$ and $\delta\boldsymbol{S}_j(t) \equiv \boldsymbol{S}_j(t) - \boldsymbol{S}_j^f$. The above coupled differential equation can be solved by Laplace transform: $\mathcal{L}[f(t)] \to \bar{f}(s)$. In the thermodynamic and the weak-coupling limit, we arrive at the final form of $\overline{\delta\Delta}(s)$:

$$\overline{\delta\Delta}(s) = \frac{\delta\Delta_0}{2\Delta_{0f}}\left(\frac{1}{\left(\frac{s}{2\Delta_{0f}}\right)} - \frac{1}{\left[\left(\frac{s}{2\Delta_{0f}}\right)^2 + 1\right]\tan^{-1}\left(\frac{s}{2\Delta_{0f}}\right)}\right). \tag{9}$$

By inverse Laplace transform, we get the approximate form of $\Delta(t)$ (see Appendix A):

$$\Delta(t) \approx \Delta_f + 2\delta\Delta_0 \frac{\cos 2\Delta_f t}{\ln 4\Delta_f t}. \tag{10}$$

B. Doping cases

In the high-doping limit ($\mu \gg \Delta_{0f}$) as illustrated in Fig. 1(d), the system without attractive interaction is basically a normal metal; therefore, we expect the Higgs mode will have the square-root decaying behavior. To verify this, we choose $\mu = 0.12 = 10\Delta_{0f}$ and simulate Eqs. (4)–(6) with other parameters equal to those in the half-filled case. The result is shown in Appendix B. We can that see $|\Delta(t)|$ indeed decays as $1/\sqrt{t}$, with the oscillation frequency equal to $2\Delta_\infty$.

To see how the mode change from the logarithmic decay to the $1/\sqrt{t}$ decay, we investigate the low-doping limit where $\mu \sim \Delta_{0f}$ [Fig. 1(e)]. By simulating Eqs. (4)–(6) with several different values of μ, we find that there are two frequencies in the low-doping case: one is the Higgs frequency $2\Delta_\infty$, and the other is slightly larger than the first one, resulting in a beat pattern as shown in Fig. 4(a). As μ increases, we find

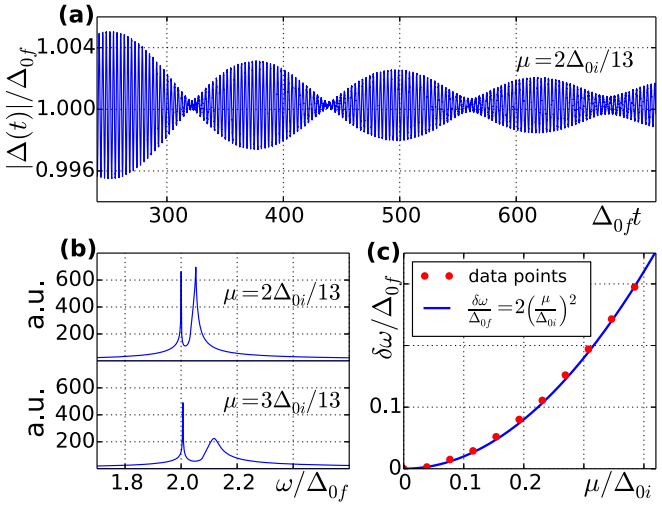

FIG. 4. Low-doping case. The quench parameters are the same as in Fig. 2. (a) The two slightly different frequencies give rise to a beat pattern of the amplitude mode. (b) The frequencies obtained by discrete Fourier transform (DFT) of $|\Delta(t)|$. Both frequencies increase as μ increases, while the larger one increases more noticeably. Besides, the larger-frequency peak also broadens and will eventually disappear as μ increases, accomplishing the gradual transform from logarithmic decay to square-root decay. (c) The frequencies data (red dots) collect by DFT of different values of μ, they fit quite well by the empirical formula (blue line).

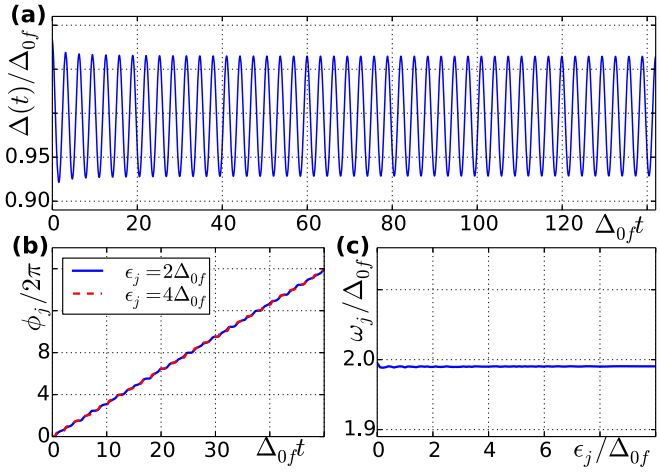

FIG. 5. 3D Dirac semimetal case. The quench parameters are equal to those in Fig. 2. (a) The Higgs mode shows an undamped oscillation. (b) Precession phase of a single spin on energy levels $\epsilon_j = 2\Delta_{0f}, 4\Delta_{0f}$. (c) The precession of different pseudospins synchronize.

that both frequencies increase. However, the Higgs frequency increases only slightly, while the lager frequency increases more remarkably and the peak broadens [Fig. 4(b)]. Physically, the decay of the Higgs mode is due to its interaction with the bottom part of the particle-hole continuum [11,24]. As we doped away from half filling, those states most responsible for the damping increase, resulting a faster-decaying behavior. When μ is large enough (about $2\Delta_{0f}$), the second peak can hardly be discerned and the transform from the logarithmic decay to square-root decay is accomplished. We also find a very interesting empirical formula, associating the difference of the two frequencies $\delta\omega$ with the chemical potential μ as $\frac{\delta\omega}{\Delta_{0f}} = 2(\frac{\mu}{\Delta_{0i}})^2$.

IV. DIRAC SEMIMETAL CASE

We extend our calculation to the 3D Dirac semimetal case. The DOS is proportional to ϵ^2 when the Fermi level is on the Dirac point. We numerically solve the collective motion of pseudospins with all the parameters equal to those in the half-filled honeycomb-lattice case. We find that the Higgs amplitude mode in this case exhibits an undamped oscillation as shown in Fig. 5(a). To explain this, we study the phase dynamics $\phi_j(t)$ of each pseudospin $\boldsymbol{S}_j(t)$ that precesses around its own time-independent vector $\boldsymbol{b}_j^{\infty}$. From Figs. 5(b) and 5(c), we can see that all the pseudospins precess with the same angular frequency $2\Delta_{\infty}$. Therefore, for the two instances of time separated by $T = \pi/\Delta_{\infty}$, the whole pseudospin configuration is identical. Since $\Delta(t)$ depends explicitly on the sum of the x components of all the pseudospins, it must be periodic and undamped. Compared with the 2D case at half filling, the particle-hole continuum most responsible for the damping consists of an even smaller fraction of the whole phase space. Therefore, the damping originating from the interaction with those states is negligible. We note that the above discussion is for the singlet-pairing case. However, triplet pairing is also possible, which has three independent Higgs mode [25]. Studying the time evolution of these Higgs modes would also be interesting.

V. DISCUSSION AND SUMMARY

For the 2D superconducting Dirac fermion case, the quenched process can be realized on two-component cold Fermi gases trapped in a honeycomb optical lattice [17], with an attractive Hubbard U tunable by the Feshbach resonance [18]. The Higgs mode in this case can be detected with rf-absorbtion techniques [26,27]. As for the Higgs amplitude mode in the 3D case, the observation is made possible by the recent discovery of superconductivity in Dirac semimetals [19,20], together with the development of the ultrafast THz pump-probe spectroscopy [28]. In principle, the measurement should be similar to the already discovered Higgs mode in clean NbN films [6]. One can use an intense monocycle THz pump pulse to generate the Higgs amplitude mode in the superconducting Cd_3As_2 thin film. Immediately after that, a probe pulse also irradiates the sample. By measuring the pump-probe delay time and the wave form of the transmitted probe pulse, one can resolve the time evolution of the Higgs mode inside the sample [6,7].

In summary, we find the Higgs amplitude mode in a half-filled honeycomb lattice has a logarithmic decaying behavior. It can be understood by studying its phase dynamics and by analytically solving the linearized equations of motion. The dynamics of doped cases in honeycomb lattice is also studied. As for the three-dimensional Dirac semimetal case, we find that the Higgs mode exhibits an undamped oscillation when the Fermi level is at the Dirac point.

ACKNOWLEDGMENT

This work was financially supported by NBRP of China (2012CB821402 and 2015CB921102) and NSF-China under Grants No.11534001, No. 11504008, and No. 11304280.

APPENDIX A: INVERSE LAPLACE TRANSFORM OF EQ. (9)

By doing the Laplace transform of the linearized equations of motion, we get the following equation for $\overline{\delta\Delta}(s)$ up to linear order in $\delta\Delta_0$:

$$\overline{\delta\Delta}(s)\sum_j \frac{1}{\left(s^2+4\Delta_{0f}^2+4\epsilon_j^2\right)\left(\Delta_{0f}^2+\epsilon_j^2\right)^{\frac{1}{2}}} = \frac{s\delta\Delta_0}{s^2+4\Delta_{0f}^2}\sum_j \frac{\epsilon_j^2}{\left(s^2+4\Delta_{0f}^2+4\epsilon_j^2\right)\left(\Delta_{0f}^2+\epsilon_j^2\right)^{\frac{3}{2}}}. \tag{A1}$$

In the thermodynamic limit and weak-coupling limit, we have $\sum_j f(\epsilon_j) \propto \int_0^{\omega_D} f(\epsilon)\epsilon d\epsilon \approx \int_0^{\infty} f(\epsilon)\epsilon d\epsilon$. After integration, we get Eq. (9) in the main text.

By using the similarity theorem $\mathcal{L}^{-1}[f(\bar{s}/a)] = af(at)$, we need only find the inverse Laplace transform of $\bar{f}(s) = 1/(s^2+1)\tan^{-1}s$. We achieve this by evaluating the Bromwich integral:

$$f(t) = \frac{1}{2\pi i}\int_{\gamma-i\infty}^{\gamma+i\infty} ds\,\bar{f}(t)e^{st}, \tag{A2}$$

where γ should be larger than the real part of any poles in the integrand.

We choose the contour shown in Fig. 6 and use Cauchy's integral theorem to evaluate the Bromwich integral C_0 marked in blue. Jordan's lemma tells us that the contributions from big arcs Γ_1,Γ_2, Γ_3 are zero, and it is easy to verify that the integrals along the small arcs γ_1 and γ_2 have no contributions,

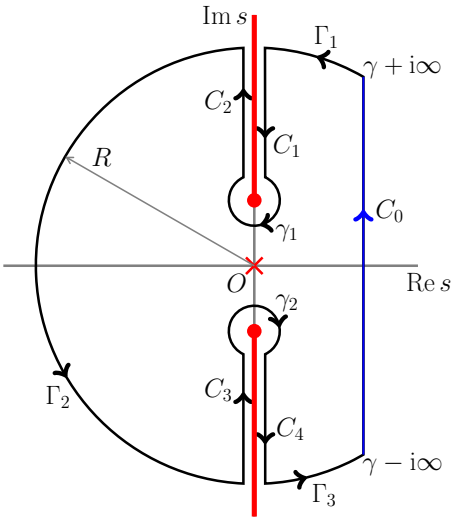

FIG. 6. The contour of the integral. The red cross represents the pole at $s=0$, the red points are branch points at $s=\pm i$, the red lines are the two branch cuts.

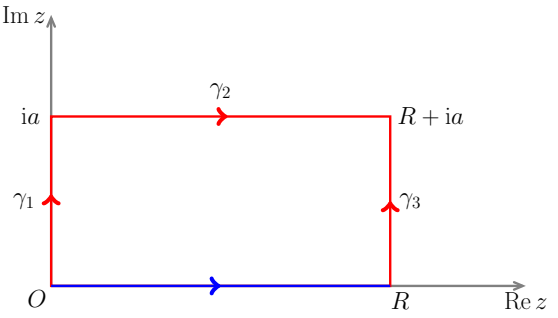

FIG. 7. The contour for $I_2(t)$. a is a small real positive number, the integral $I_2(t)$ (blue) is replaced by the contour in red, while integration along γ_2 and γ_3 gives zero.

either. The only remaining parts are the pole at the origin and line integrals C_1 to C_4. So we have

$$f(t) = \theta(t) - 4I_2(t), \tag{A3}$$

$$I_2(t) = \mathrm{Re}\left[e^{it}\int_0^{\infty}\frac{e^{ixt}}{(x^2+2x)\left[\left(\ln\frac{x}{x+2}\right)^2+\pi^2\right]}dx\right]. \tag{A4}$$

We use the contour in Fig. 7 to evaluate Eq. (A4), and the only remaining contribution is from the line integral γ_1. To the leading order, we have:

$$I_2(t) = \mathrm{Re}\left[e^{it}\int_0^{2a}\frac{e^{-2yt}}{2y(\ln y)^2}dy\right]. \tag{A5}$$

For sufficiently large t, the above integral can be calculated by using a result by Erdélyi [29]; thus we obtain Eq. (10) in the main text.

APPENDIX B: HIGH-DOPING-LIMIT CASE

We choose $\mu = 0.12$ in this case. Because the exact particle-hole symmetry is absent when $\mu \neq 0$, $\Delta(t)$ will acquire a time-depended phase during the evolution; thus we plot the amplitude $|\Delta(t)|$ in the Fig. 8. We fit the data by using the following equation provided in many publications [9,11,13]:

$$\frac{|\Delta(t)|}{\Delta_{0f}} = a + \frac{2b\delta\Delta_0}{\pi^{\frac{3}{2}}\Delta_{0f}\sqrt{\Delta_{0f}t}}\cos\left(c\Delta_{0f}t + d\frac{\pi}{4}\right). \tag{B1}$$

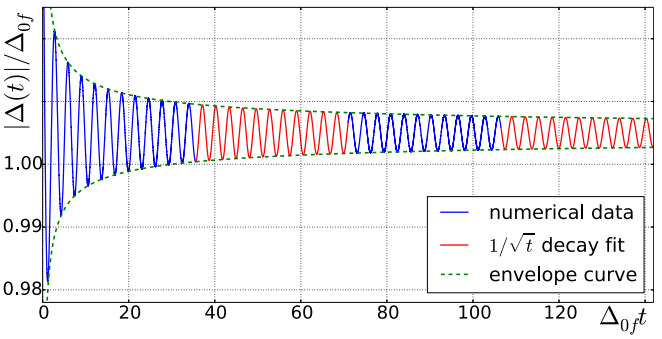

FIG. 8. High-doping limit with $\mu = 0.12$; other parameters are same as those in Fig. 2 in the main text. The numerical data (blue) are well fit by Eq. (B1).

The fitting parameters are $a = 1.0050$, $b = 0.5142$, $c = 2.0101$, $d = 0.9827$. We see $c = 2a$ is almost exactly satisfied, indicating that this is the Higgs amplitude mode. However, a is slightly greater than 1, meaning Δ_∞ is slightly greater than Δ_{0f}. This is not so surprising because the relation $\Delta_\infty \approx \Delta_{0f} - \delta\Delta_0^2/6\Delta_{0f}$ is obtained under the condition of strictly constant density of states. In conclusion, in the high-doping limit, the system behaves as a normal metal without interactions, resulting in the $1/\sqrt{t}$-decaying property of the amplitude $|\Delta(t)|$.

[1] D. Pekker and C. M. Varma, Annu. Rev. Condens. Matter Phys. **6**, 269 (2015).
[2] P. W. Anderson, Phys. Rev. **130**, 439 (1963).
[3] P. W. Higgs, Phys. Lett. **12**, 132133 (1964).
[4] M. Greiter, Ann. Phys. (NY) **319**, 217 (2005).
[5] A. Pashkin, and A. Leitenstorfer, Science **345**, 1121 (2014).
[6] R. Matsunaga, Y. I. Hamada, K. Makise, Y. Uzawa, H. Terai, Z. Wang, and R. Shimano, Phys. Rev. Lett. **111**, 057002 (2013).
[7] R. Matsunaga, N. Tsuji, H. Fujita, A. Sugioka, K. Makise, Y. Uzawa, H. Terai, Z. Wang, H. Aoki, and R. Shimano, Science **345**, 1145 (2014).
[8] D. Sherman, U. S. Pracht, B. Gorshunov, S. Poran, J. Jesudasan, M. Chand, P. Raychaudhuri, M. Swanson, N. Trivedi, A. Auerbach, M. Scheffler, A. Frydman and M. Dressel, Nat. Phys. **11**, 188 (2015).
[9] N. Tsuji and H. Aoki, Phys. Rev. B **92**, 064508 (2015).
[10] P. B. Littlewood and C. M. Varma, Phys. Rev. B **26**, 4883 (1982).
[11] A. F. Volkov and Sh. M. Kogan, Zh. Eksp. Teor. Fiz. **65**, 2038 (1973) [Sov. Phys. JETP **38**, 1018 (1974)].
[12] R. A. Barankov and L. S. Levitov, Phys. Rev. Lett. **96**, 230403 (2006).
[13] E. A. Yuzbashyan and M. Dzero, Phys. Rev. Lett. **96**, 230404 (2006).
[14] P. R. Wallace, Phys. Rev. **71**, 622 (1947).
[15] S. M. Young, S. Zaheer, J. C. Y. Teo, C. L. Kane, E. J. Mele, and A. M. Rappe, Phys. Rev. Lett. **108**, 140405 (2012).
[16] N. B. Kopnin and E. B. Sonin, Phys. Rev. Lett. **100**, 246808 (2008).
[17] L. Tarruell, D. Greif, T. Uehlinger, G. Jotzu, and T. Esslinger, Nature (London) **483**, 302 (2012).
[18] T. Esslinger, Annu. Rev. Condens. Matter Phys. **1**, 129 (2010).
[19] H. Wang, H. Wang, H. Liu, H. Lu, W. Yang, S. Jia, X. Liu, X. Xie, J. Wei and J. Wang, Nat. Mater. **15**, 38 (2016).
[20] L. Aggarwal, A. Gaurav, G. S. Thakur, Z. Haque, A. K. Ganguli, and G. Sheet, Nat. Mater. **15**, 32 (2015).
[21] P. W. Anderson, Phys. Rev. **112**, 1900 (1958).
[22] S. Tsuchiya, R. Ganesh, and T. Nikuni, Phys. Rev. B **88**, 014527 (2013).
[23] E. A. Yuzbashyan, M. Dzero, V. Gurarie, and M. S. Foster, Phys. Rev. A **91**, 033628 (2015).
[24] R. A. Barankov, L. S. Levitov, and B. Z. Spivak, Phys. Rev. Lett. **93**, 160401 (2004).
[25] B. Rosenstein, B. Ya. Shapiro, and I. Shapiro, Phys. Rev. B **92**, 054503 (2015).
[26] M. Dzero, E. A. Yuzbashyan, B. L. Altshuler, and P. Coleman, Phys. Rev. Lett. **99**, 160402 (2007).
[27] C. Chin *et al.*, Science **305**, 1128 (2004).
[28] T. Kampfrath, K. Tanaka, and K. A. Nelson, Nat. Photonics **7**, 680 (2013).
[29] A Erdélyi, Arch. Ration. Mech. Anal. **7.1**, 1 (1961).